River Flow 2020 – Uijttewaal et al (eds)

Study on riverbed variation management by groin at a river confluence associated with the barrage water

Y. Okamoto
Graduate School, NAGOYA UNIVERSITY Civil and Environmental Engineering, Aichi, Japan

J. Nishio
Advanced Course of Architecture and Civil Engineering, National Institute of Technology, Akashi College, Hyogo, Japan

K. Kanda
Civil Engineering, National Institute of Technology, Akashi College, Hyogo, Japan

K. Michioku
Department of Civil and Environmental Engineering, Faculty of Engineering and Design, Hosei University, Tokyo, Japan

F. Nakamura
Department of Civil and Environmental Engineering, Nagaoka University of Technology, Niigata, Japan

H. Kubo
CTI Engineering Co. Ltd., Japan

ABSTRACT: The Kakogawa River, which has a catchment area of 1730 km^2 and a length of 96.0 km, flows through Hyogo Prefecture in Japan. The influence of runoff due to barrage water and the Mino River tributary, combined with a meander in the river upstream from the large barrage on the Kakogawa River (Kakogawa Barrage), has promoted the development of a sandbar on the riverbank opposite the confluence. This sandbar, which has enlarged and become fixed, currently deflects the passage of water back to the left bank and has decreased the river's usable water-surface area. To wash away the sandbar, a groin was installed in 2015. The purpose of this study was to survey the river's topography in the vicinity of the Mino River confluence and identify the factors responsible for sandbar development using model experiments and numerical analysis. In addition, the function of the groin and the effects of changing its characteristics were verified.

1 BACKGROUND

1.1 *Introduction*

In the Kakogawa River, a first-class river in Hyogo Prefecture, a sandbar opposite the confluence of the Kakogawa and Mino Rivers has developed and expanded, causing a lowering of the discharge capacity, after the construction of a large barrage (Kakogawa Barrage) and river modifications in 1989. Briefly, the increase in the angle of confluence caused an increase in the deposition and dead-water area downstream from the confluence, which in turn caused the development of a sandbar. Because sandbar development opposite a confluence is rare, it is necessary to verify the mechanism of this sandbar's development in order to manage the river. The factors affecting the formation of the river's topography are as follows (T. Okuyama, et al., 2014.).

1) Right-angled meander in the river upstream from the confluence
2) Right-angled tributary in the Mino River
3) Backwater from the large Kakogawa Barrage

In addition, a groin was installed upstream from the confluence to suppress the development of a sandbar on the right side of the riverbank, making the flow more complex. There are a few proper examples of groins installed in a confluence, so it seems that clarifying the characteristics of the flow and riverbed variation caused by the groin is important to the riverbed variation management in actual river.

A previous study (S. Takata, et al., 2017) clarified the influence of meanders, barrage height, and the ratio of flow discharge using a model experiment and numerical analysis. Therefore, the purpose of this study was to verify the function of the groin and survey the effects caused by changing the its shapes of the groin during flood and normal flow conditions. To verify the reproducibility of the experimental results, we conducted numerical calculations using flow-analysis software, iRIC (International River Interface Cooperative, 2013), and we investigated how the software can be applied.

1.2 *Overview of the confluence*

The Kakogawa River, which has a catchment area of 1730 km^2 and a length of 96.0 km, flows through Hyogo Prefecture in Japan. The Mino River, which has a catchment area of 304 km^2 and a length of 39.0 km, flows at a right angle to the Kakogawa River. The confluence of the two rivers is 15.8 km from the estuary (**Figure 1**). Around the confluence, the width of the main channel is nearly 200 m and its slope is about 1/850. The width of the tributary channel is nearly 120 m and its slope is about 1/500; however, the influence of the tributary channel's slope can be ignored because a falling work with a height of 2 m was installed upstream of the Mino River, before the confluence. In 1989, the Kakogawa Barrage was constructed 12.0 km from the estuary to improve the reliability of flood control and to respond to the rapidly increasing demand for water. In normal times, the backwater caused by the barrage affects the upstream of the confluence.

Figure 1. Aerial photograph of the site.

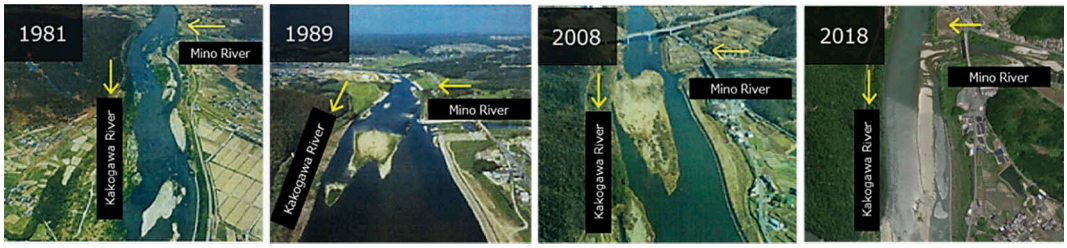

Figure 2. Morphological changes in the confluence.

Figure 2 shows the morphological changes in the confluence before and after construction of the barrage and groin. At the same time as the construction of the barrage, upstream river modifications were made, which promoted the development of a sandbar opposite the confluence. In 1981, before the barrage was constructed, the main flow area was on the right side of the river. However, in 1990, after the barrage was constructed, the main flow area had moved to the left because of the sandbar. Furthermore, the upstream river channel of the confluence has a right-angled meander 18 km from the estuary, and a narrow segment was formed due to protruding bedrock on the left bank of the low-water channel at 16.7 km from the estuary. It is considered that the development of the sandbar in the confluence has been influenced by the meander upstream of the Kakogawa River, the backwater from the Kakogawa Barrage, and the Mino River tributary.

In 2015, a groin was installed to control the development of the sandbar just upstream of the confluence. This groin was made by block stacking, and it is 50 m long, 15 m wide, and 6 m high. It aims to manage the sandbar by deflecting the main flow toward the right bank during flooding, but the function of the groin has not been adequately verified. Now, the sandbar has been flushed by the groin, but a new sandbar is developing behind the groin, and a small deposition can be observed in front of the groin.

2 METHODOLOGY OF THE STUDY

2.1 *Model experiment*

Figure 3 shows the study's model experimental channel, which is rectangular and reproduces the river channel of the site using a scale of 1:250. The main channel is 8 m long, 0.8 m wide, and 0.4 m deep, and the tributary channel is 0.4 m wide and joins the left bank of the main channel at a right angle 4.33 m downstream from the upstream part of the main channel. The slope of the channel is set as 1/850, which is similar to the slope of the site. In the tributary, the falling work, which hight is 8 mm, was installed 0.45 m upstream from the confluence to simulate the local river channel. In the coordinate system, the X-axis is the flow direction, the Y-axis is the width direction, and the Z-axis is the vertical direction. The origin is on the right bank, 1.5 m downstream from the upstream part of the main channel, and it is 0.1 m above

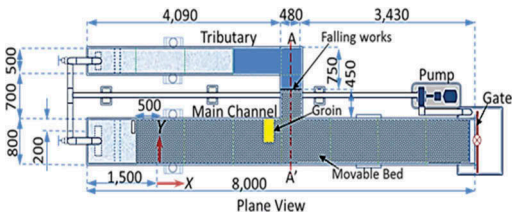

Figure 3. Experimental channel.

the bottom of the channel. The center line of the tributary channel is on the traverse line of X = 2.83 m. The water surface is controlled by the movable barrage of the rise-and-fall system that was installed downstream from the main channel. Table 1 shows the conditions. Case A targets the flood flow rate, and the case of Q_m = 5.0 l/s reproduces the conditions of the largest flow rate at the site. Case B targets the site's normal flow rate. In the preliminary experiment for normal flow conditions, the amount of riverbed variation was very small under the same flow ratio as for flood conditions. Based on that, we set the flow ratio at 0.5 for normal flow conditions. Furthermore, we installed two types of groins (**Figure 4**) at right angles to the flow direction before the confluence on the right bank of the main channel (X = 2.35 m). The normal-type groin reproduced the shape of the groin in the field. This groin is impermeable and overflow. The slit-type groin changed the characteristics of this normal-type groin to permeable and non-overflow. For the riverbed material, we used two sizes of coal powder: a small size that corresponded to the normal flow rate and a large one that corresponded to the flood flow rate.

Table 2shows the characteristics. To prevent the occurrence of sand waves, we chose coal powders having a grain size larger than 1/850 of the average grain size of the riverbed material at the site, and both coal powders corresponded to the largest grain size of the riverbed at the site. Accordingly, a similarity low of sediment transport was reproduced by matching the ratio of the

Table 1. Conditions of this study.

No.	Time T(h)	Discharge of Main Flow Q_m (ℓ/s)	Discharge of Tributary Flow Q_t (ℓ/s)	Target Flow	Barrage height D(cm)	Groin
CaseA-1						No
CaseA-2	1.0	5.0	1.0	Flood	0.0	Normal
CaseA-3						Slit
CaseB-1						Normal
CaseB-2	1.0	0.8	0.4	Normal	0.0	Slit

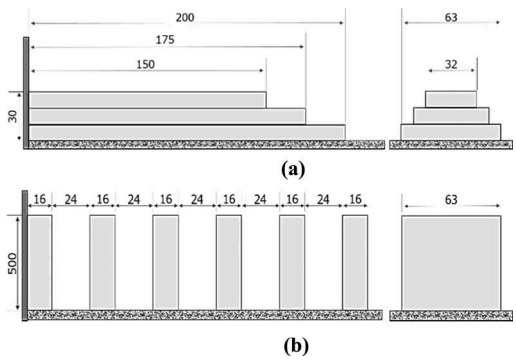

Figure 4. Shapes of the groins (a: Normal, b: Slit).

Table 2. Characteristics of riverbed materials.

Target Flow	Flood	Normal
Density ρ_s (g/cm^3)	1.47	1.47
Average Particle Diameter (mm)	1.3	0.9
Critical Friction Velocity U_{*c} (cm/s)	1.44	1.20

friction velocity to the critical friction velocity between the riverbed material at the site and the coal powder. As an initial setting, we spread the coal powder 0.1 m high over the entire surface of the main channel and downstream of the falling work in the tributary channel. For the upstream conditions, a board 0.2 m wide was installed at the right bank of the main channel (X = -0.5 m) to reproduce the influence of the meander. The study did not consider the sand feeding from the river upstream because the ratio of the sand feeding between the main river channel and the tributary at the site was unclear. In the experiment, we measured the velocity of the water surface and the vector. The former was measured using the LSPIV method (I. Fujita, 1998). After the water was drained, we measured the riverbed variation using a laser range finder.

2.2 *Numerical calculations*

To verify the results of the experiment, we conducted numerical calculations using iRIC Software[4]. We used two solvers: Nays2DH for 2-D analysis and NaysCUBE for 3-D analysis. Both solvers were developed by the International River Interface Cooperative (IRIC) and released on the internet.

2.2.1 *Summary of Nays2DH*

The formulae for Nays2DH are as follows. Formula (1) presents the equation of continuity on the plane's rectangular coordinate. Formulae (2) and (3) present equations of motion in the x and y directions. Finally, formula (4) presents the continuity equation of sediment transport. The formulae were converted to the generalized coordinate system, and the iRIC program calculates by using the converted formulae. The Cubic Interpolated Profile (CIP) method was used to discretize the diffusion terms, and the k-model was applied to the turbulent-flow field. The equation of bed-load transport used in this software was developed by Mr. Ashida and Mr. Mitiue.

$$\frac{\partial h}{\partial t}+\frac{\partial (uh)}{\partial x}+\frac{\partial (vh)}{\partial y}=0 \tag{1}$$

$$\frac{\partial (uh)}{\partial t}+\frac{\partial \left(hu^2\right)}{\partial x}+\frac{\partial (huv)}{\partial y}=-hg\frac{\partial H}{\partial x}-\frac{\tau_x}{\rho}+D_x \tag{2}$$

$$\frac{\partial (vh)}{\partial t}+\frac{\partial (huv)}{\partial x}+\frac{\partial \left(hv^2\right)}{\partial y}=-hg\frac{\partial H}{\partial y}-\frac{\tau_y}{\rho}+D_y \tag{3}$$

$$\frac{\partial z}{\partial t}+\frac{1}{1-\lambda}\left(\frac{\partial q_{bx}}{\partial x}+\frac{\partial q_{by}}{\partial y}\right)=0 \tag{4}$$

where, x, y: plane rectangular coordinate; u, v: mean velocity of the x, y directions; t: time (sec); h: water depth; H: elevation of the water surface; g: gravitational acceleration (m/s^2); ρ: water density; τ_x, τ_y: sheer force of the x, y directions (kg/m/s^2); D_x, D_y: diffusion term; z: height of the riverbed; l: porosity; q_{bx}, q_{by}: bed-load transport of the x, y directions (m^2/s).

2.2.2 *Summary of NaysCUBE*

The formulae for NaysCUBE are as follows. Formula (5) presents the equation of continuity on the Cartesian coordinate system. Formula (6) presents the equations of motion in the three dimensions. Formulae (7) and (8) present the k-equation and ε-equation, respectively. The formulae were converted to the generalized curvilinear-coordinate system, the iRIC program calculates by using diffusion terms, and the k-model was applied to the turbulent-flow field.

$$\frac{\partial U^i}{\partial x^i}=0 \tag{5}$$

$$\frac{\partial U^i}{\partial t} + \frac{\partial U^i U^j}{\partial x^j} = G^i - \frac{1}{\rho}\frac{\partial p}{\partial x^i} + \frac{\partial\left(-\overline{u^i u^j}\right)}{\partial x^j} + v\frac{\partial^2 U^i}{\partial x^i \partial x^j} \tag{6}$$

$$\frac{\partial k}{\partial t} + \frac{\partial k U^j}{\partial x^j} = -\overline{u^i u^j}\frac{\partial U^i}{\partial x^j} - \varepsilon + \frac{\partial}{\partial x^j}\left\{\left(\frac{v_t}{\sigma_k} + v\right)\frac{\partial k}{\partial x^j}\right\} \tag{7}$$

$$\frac{\partial \varepsilon}{\partial t} + \frac{\partial \varepsilon U^j}{\partial x^j} = -C_{\varepsilon 1}\frac{\varepsilon}{k}\overline{u^i u^j}\frac{\partial U^i}{\partial x^j} - C_{\varepsilon 2}\frac{\varepsilon^2}{k} + \frac{\partial}{\partial x^j}\left\{\left(\frac{v_t}{\sigma_\varepsilon} + v\right)\frac{\partial \varepsilon}{\partial x^j}\right\} \tag{8}$$

where, x^i: spatial coordinates; t: time; U_i: flow velocity; p: pressure; u^i: turbulent velocity; v: kinematic viscosity coefficient; ρ: fluid density; k: turbulent kinematic energy; ε: dissipation rate of turbulent kinematic energy; v_t: turbulent kinematic viscosity coefficient; G^i: gravity acceleration; $-\overline{u^i u^j}$: Reynolds stress tensor.

2.2.3 *Other conditions*

The experimental channel was reproduced using this software, and the mesh was generated at a 2-cm pitch. The conditions were set based on those of the experiment. For the boundary condition, we used the flow rate at the upstream part of the main and tributary channels. The amount of sand feeding was zero in both channels. The water elevation in the downstream part of the channel was given as the sum of the height of the barrage and the critical depth. The roughness coefficient was set as $n = 0.018$ m$^{1/3}$/s. Because of the high computational load, in the three-dimensional (3-D) analysis, the riverbed variation was calculated only around the groin.

3 RESULTS AND CONSIDERATIONS

3.1 *Results for water surface velocity*

Figure 5 shows the results regarding the water surface velocity in flood conditions. In Case A-1, the maximum flow velocity was observed downstream from the confluence, and a dead-water zone was observed near the left bank, behind the confluence. However, in Case A-2, the maximum flow velocity area moved to the right bank due to installation of the groin. The dead-water zone after the confluence decreased, but the area around the groin also became a dead-water zone because the groin greatly changed the flow. In Case A-3, a slit-type groin was installed. In the results, the maximum flow velocity was observed in the same area as in Case A-2. Because water can flow through the slit-type groin, the vectors of this flow were

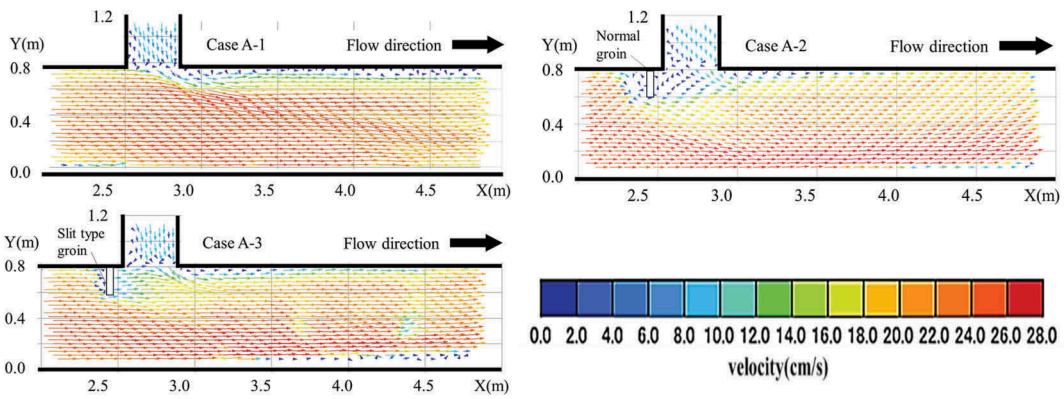

Figure 5. Water surface velocity (Cases A-1 & A-2&A-3).

observed behind the groin, and there was no dead-water zone behind it. Based on these results, each groin can change the main flow area to the right bank. The occurrence of the dead-water zone around the groin depends on the shape of the groin, which determines whether water can flow through the groin or not.

3.2 *Experimental results for flood flow*

Figure 6 shows the results regarding riverbed variation in flood conditions. In Case A-1, riverbed degradation occurred along the tributary flow, and deposition occurred in the middle of the channel near the confluence. It seems that this sandbar reproduces the actual topography of the site, but the position actually differs from that at the site. We think this difference is caused because we did not consider the sand feeding by the tributary flow. Downstream from the confluence, the deposition occurred near the left bank. The results for Case A-2 showed the effects of riverbed variation with the installation of a normal-type groin. In Case A-2, riverbed degradation occurred near the right bank after the confluence because the groin deflected the flow toward the right bank before the confluence. When this flow was sharply deflected by the groin, a secondary wave occurred in front of the groin, the flow from which caused deep scouring in front of the groin. In contrast, deposition developed behind the groin, preventing the flow of the tributary. Unlike in Case A-1, no deposition near the confluence was observed in Case A-2. Accordingly, the groin can flush the sandbar but also promotes the development of a new sandbar behind the groin.

The results of Case A-3 show the riverbed variation with the installation of a slit-type groin. Because a slit-type groin is a transmission-type one, the deflection effect was diminished and the scouring area in front of the groin decreased in comparison with the results of Case A-2. The deposition area and its height also decreased. Riverbed degradation was observed near the right bank, so it is considered that the slit-type groin has a flushing effect like that of the normal-type groin and that deposition behind the groin can be reduced by using a slit-type groin.

3.3 *Experimental results for normal flow*

Figure 7 shows the results of riverbed variation under normal flow conditions in the presence of groins. In Case B-1, the tendency of the riverbed variation differed from that in Case A-2. No deep scouring was observed in front of the groin, but scouring instead occurred locally at the groin's tip. However, like at the site, deposition occurred in front of the groin. As in Case

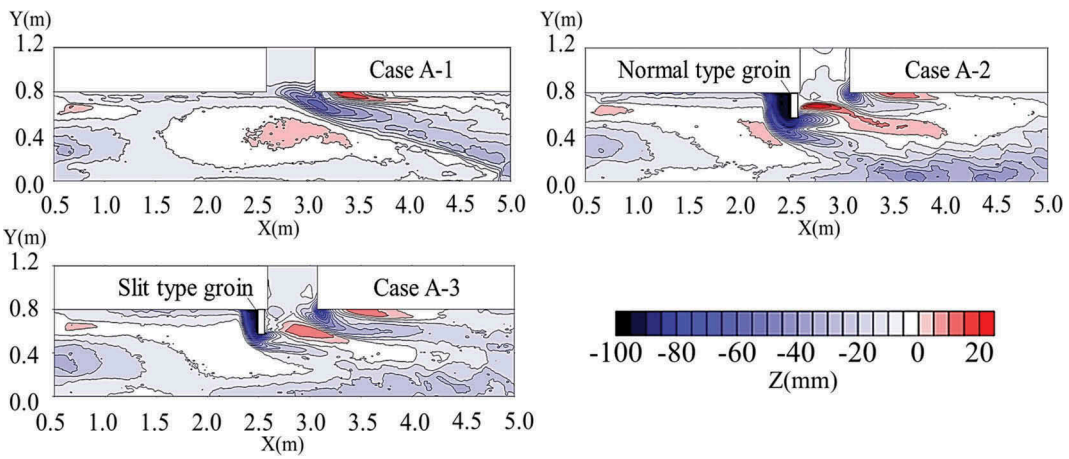

Figure 6. Experimental results for riverbed variation (Cases A-1, A-2, & A-3).

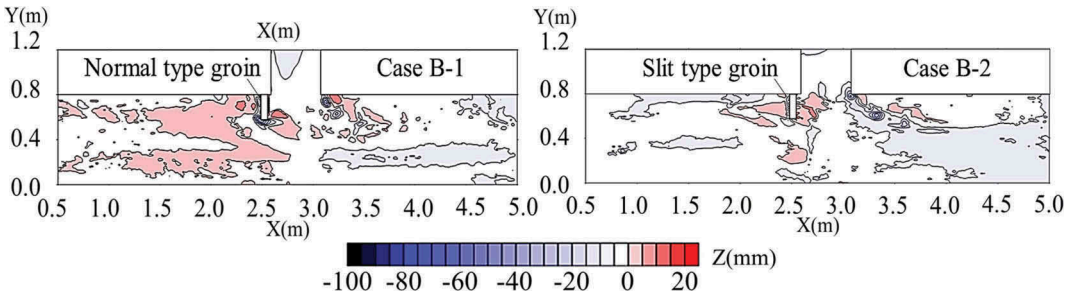

Figure 7. Experimental results for riverbed variation (Cases B-1 & B-2).

A-2, riverbed degradation occurred near the right bank, after the confluence, and deposition developed behind the groin. Accordingly, it seems that regardless of the flow conditions, the normal-type groin also has a flushing effect and promotes the development of a sandbar behind the groin.

The results regarding Case B-2 showed the riverbed variation with the slit-type groin installed and under conditions of normal flow. Riverbed degradation along the tributary flow was observed. As in Case B-1, deposition occurred around the groin; however, the area, including its height, were smaller than in Case B-1. In Case B-2, no riverbed variation was caused by the deflected flow downstream from the groin. Therefore, the slit-type groin demonstrated a low flushing effect.

However, this groin was more effective than the normal-type groin in reducing the development of a sandbar behind the groin in normal flow conditions.

3.4 *Results of numerical analysis*

3.4.1 *2-D analysis*

Figure 8 shows the results of the numerical calculations using the iRIC Nays2DH. In these results, the effect of using the board as the upstream boundary condition were stronger than in the experimental results, resulting in deposition developing from the left bank of the upstream part to the middle of the channel. In the absence of a groin, the tendency regarding riverbed variation was the same as in the experiment. Installation of the groin reproduced the

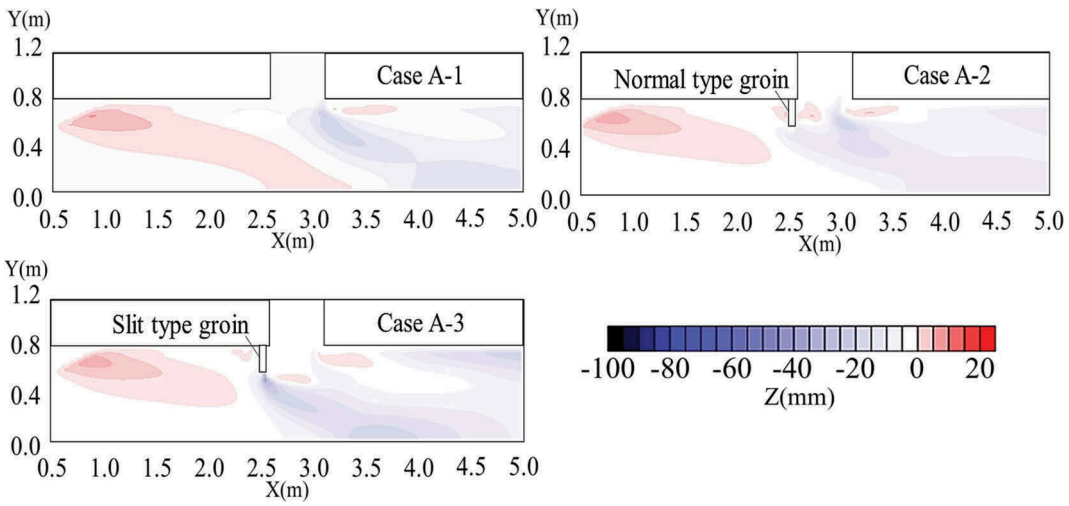

Figure 8. 2-D analysis results for riverbed variation (Cases A-1, A-2, & A-3).

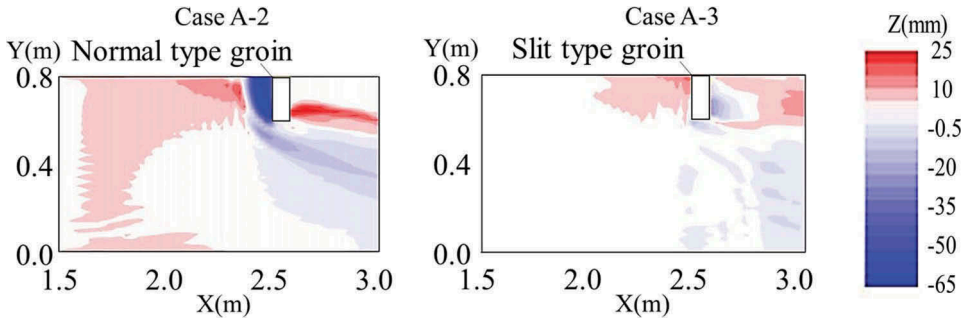

Figure 9. 3-D analysis results for riverbed variation (Cases A-2 & A-3).

scouring at the tip of the groin and the riverbed degradation near the right bank, after the confluence. However, the deep scouring in front of the groin was not observed. It seems that deep scouring was caused 3-D analysis

Figure 9 shows the results of 3-D analysis using the iRIC NaysCUBE. In Case A-2, the deep scouring in front of the groin and the deposition behind the groin were the same as those in the experimental results. In Case A-3, deposition occurred in front of the groin, and shallow scouring occurred behind it. This was caused by the influence of the width of the transmission parts. In the calculation, the slit-type groin was reproduced using an obstacle cell. Therefore, because of the pitch of the calculation mesh, the width of the transmission parts was smaller than the width of the real ones. Based on that, it seems that the condition needs to be modified.

4 CONCLUSIONS

The study's conclusions are as follows.

(1) In the flood condition, a variation in riverbed degradation occurs along the tributary flow, and a deposition-like sandbar occurs in the site in the middle of the channel near the confluence.
(2) The normal-type groin can flush the deposition that produces the sandbar. However, a deposition develops behind the groin, and deep scouring occurs in front of it. Measures against these problems are needed. A slit-type groin can reduce the riverbed variation around the groin and retain the flushing effect.
(3) In the normal flow condition, no deposition is observed near the confluence. However, degradation is observed along the tributary, as it is in the results regarding the flood condition.
(4) Both types of groin retain the flushing effect in the normal flow condition. However, a small deposition occurs in front of the groin. This deposition is also observed at the site.
(5) Numerical calculations using the iRIC software can reproduce the experimental results under the condition in which no groin is installed. In the case in which a groin is installed, the numerical calculation cannot reproduce the river bed variation around the groin.
(6) In the 3-D results, the tendency of the riverbed variation around the groin is nearly the same as that in the experimental results. Based on that, it seems that the scouring occurs during flooding and that the scoured area is then filled by normal flow.

ACKNOWLEDGEMENTS

For this study, we cooperated with the Himeji office of the Ministry of Land, Infrastructure, and Transport and used a grant for a joint study from the College of Technology and Nagaoka University of Technology. We express our thanks to them.

REFERENCES

I. Fujita., 1998. Application of PIV technology to the water surface of real river, Advances in River Engineering Vol. 4, pp. 41–46.

International River Interface Cooperative, 2013. Text of training session for iRIC in KANSAI.

S. Takata, K. Kanda., K. Michioku., H. Kubo, Y. Okamoto, 2017. Bed variation and its control at a river confluence associated with the upstream river topography and release of the barrage, Proceedings of Hydraulic Engineering, JSCE Vol. 76 (No. 4), pp. 865–870.

T. Okuyama, K. Michioku, K. Kanda, S, Kometani, 2014. Numerical analysis about morphological change at river confluence associated with barrage, Advances in River Engineering Vol. 20, pp. 307–311.